Journal of Materials Chemistry C

ROYAL SOCIETY OF CHEMISTRY

PAPER

View Article Online
View Journal | View Issue

Cite this: J. Mater. Chem. C, 2024, 12, 13609

ESIPT-active columnar liquid crystal: organic dyes and quantum dots-assisted fluorescence modulation†

Shikha Agarwal, [a] Santosh Y. Khatavi, [b] Bhupendra Pratap Singh, [c] Madhu Babu Kanakala, [d] Pralay Kumar Santra, [b] Sandeep Kumar, [ef] Chi-Yen Huang, [g] Channabasaveshwar V. Yelamaggad*[bhi] and Rajiv Manohar*[a]

Tailoring, fine-tuning, and controlling the luminescent behavior and the associated photo-physical properties of fluorophores have been the subject of contemporary research. Over the years, many strategies have been explored to address concerns such as short electronic absorption/luminescence wavelengths, small Stokes shift, low brightness, inapt permeability, poor stability, and low solubility. Among these, approaches involving binary/multi-component systems comprising different functional materials appear to be promising and everlasting. Working on this theme, we report the results of elaborative studies on the fluorescence (photoluminescence, PL) characteristics of several organic/hybrid composites realized by dispersing organic dyes and quantum dots (QDs) in the host columnar liquid crystal (Col LC) exhibiting excited-state intra-molecular proton-transfer (ESIPT) phenomenon. Precisely, the binary mixtures were realized by doping organic dyes such as methyl red/rubrene and carbon QDs/perovskite ($CsPbBr_3$) QDs in fluorescent (ESIPT) Col LC, namely, phasmidic bis(*N*-salicylideneaniline) (PBSAN-14). The investigations were carried out in three condensed states, *viz.*, solid, LC, and liquid states, and their solutions. The composites derived from organic dyes and Col LC refrain from light emission, implying that the PL of the host is quenched; the Stern–Volmer profiles revealed the combined dynamic and static quenching mechanism. The Col LC-QD composites exhibit intense emission that covers almost the entire visible wavelength region. The CIE chromaticity diagram shows a wide range of color tuning achieved by varying the nature of additives. Thus, this investigation provides a clear insight into the effect of organic dyes and QDs on the condensed states of fluorophores.

Received 11th April 2024,
Accepted 9th July 2024

DOI: 10.1039/d4tc01492h

rsc.li/materials-c

[a] *Liquid Crystal Research Laboratory, Department of Physics, University of Lucknow, Lucknow, Uttar Pradesh 226007, India. E-mail: rajiv.manohar@gmail.com*
[b] *Centre for Nano & Soft Matter Sciences (CeNS), Bengaluru, India. E-mail: yelamaggad@gmail.com*
[c] *Department of Electro-Optical Engineering, National United University, No. 2, Lien-Da, Miao-Li city, Miao-Li 360, Taiwan*
[d] *Beckman Coulter Life Sciences, Bengaluru 562149, India*
[e] *Raman Research Institute, Bengaluru 560080, India*
[f] *Department of Chemistry, Nitte Meenakshi Institute of Technology (NMIT), Yelahanka, Bengaluru, India*
[g] *Graduate Institute of Photonics, National Changhua University of Education, Changhua 500, Taiwan*
[h] *Department of Chemistry, Manipal Institute of Technology, Manipal Academy of Higher Education, Manipal – 576104, India*
[i] *SJB Institute of Technology, Health & Education City, Kengeri, Bengaluru – 560060, India*

† Electronic supplementary information (ESI) available: Fig. S1: 1D intensity *vs.* 2θ profiles obtained for the $Col_h/p6mm$ phase of PBSAN-14 as a function of temperature; Table S1: periodic parameter of the host PBSAN-14 at two different temperatures; Fig. S2: molecular structure of (a) methyl red dye and (b) rubrene; Fig. S3: room-temperature absorption and photoluminescence emission spectrum of different organic and inorganic dopants used in the study; (a) MRC dye, (b) rubrene, (c) carbon QDs and (d) perovskite QDs. See DOI: https://doi.org/10.1039/d4tc01492h

1. Introduction

Excited-state intramolecular proton transfer (ESIPT) active molecules have been receiving overwhelming consideration since the first concerned report has been published by Weller, where the simultaneous existence of dual emission peaks in the photoluminescence spectrum of methyl 2-hydroxybenzoate in aprotic solvents has been reported.[1,2] Some distinctive properties such as large Stoke's shift, dual emission, ultrafast process and spectral sensitivity to the surrounding medium[3–5] have garnered significant attention to these ESIPT-active chromophores for their potential applications in a wide range of fields such as organic liquid-crystal displays, chemosensors, UV stabilizers, opto-electronic devices, laser applications, *etc.*[6–10] As per the definition, molecules that consist both proton-accepting and proton-donating groups exhibit this unique dual fluorescence emission since they are capable of undergoing proton transfer in the excited state due to an increased acidity/basicity.[11] The presence of an intramolecular hydrogen bond

between the proton donor and proton acceptor groups serves as a basic prerequisite for ESIPT activity in any system. ESIPT activity is basically a four-level photo-physical mechanism (*enol* → *enol** → *keto** → *keto*) where the molecule that exists in the ground *enol* (E) state enters into its singlet excited *enol* (E*) state upon photo-excitation. It experiences energy relaxation by tautomerization, wherein a proton transfer at an intramolecular hydrogen bonding site promotes a quick transition of an E* tautomer to its excited-state *keto* tautomer (K*). The original E tautomer is then restored by a transient reverse proton transfer that occurs after the radiative decay of K* to its electronic ground *keto* (K) state. The explanation for the dual emission is very clear; the excited state of the *keto* form, which is created by the ESIPT process, is responsible for the long wavelength emission, whereas the excited state of the *enol* form is responsible for the short wavelength emission.[12]

Modulating and enhancing the fluorescence characteristics of ESIPT molecules is crucial to achieve optimal performance as solid-state emitters, particularly from the perspective of technological applications. Researchers have explored various methods to modify the fluorescence properties of ESIPT-active molecules to enhance their utility for technological aspects including altering the ESIPT cores,[13,14] coupling ESIPT with the aggregation-induced emission (AIE) properties of luminogens,[15,16] restricting the intramolecular rotations to achieve AIE,[17] and controlling the twisted intramolecular charge transfer to prevent the fluorescence quenching.[18,19] It has been previously reported that alternations in the ESIPT cores improves the photoluminescence efficiency of the system. Moreover, these methods can help to generate color-tunable emitting materials and electroluminescent materials. An inventive method for creating white light-emitting diodes (WLEDs) is made possible by a novel nanocomposite that contains CdSe quantum dots passivated by the newly synthesized ESIPT-active molecule (HF-N-LA). This nanocomposite can produce white light and its linear color tunability can be adjusted simply by changing the relative amounts of these two species.[20] The doping of an ESIPT-active molecule C4-C≡C-HBT in 5CB has been proposed by W. Zhang *et al.* to yield highly fluorescent emission in the host NLC.[21] The effect of cyano substitution on a representative ESIPT molecule HBT has been studied by Sakurai *et al.* to enhance the quantum yield in the solid state.[22]

The introduction of several non-ESIPT active fluorescent dyes into a range of LC systems has previously been extensively documented;[21,23] nevertheless, one of the disadvantages is the steady-state absorption of the doped dyes. This reabsorption concern is not encountered by the ESIPT-active emitters intrinsically due to their large Stoke's shift.[24–27] A crucial aspect of opto-electronic applications such as luminescent solar concentrators (LSCs) and switchable holographic imaging is the transparency and emission capabilities of LC material in the visible domain.[28–31] LSCs rely on luminescent compounds placed in glass or plastic substrates to absorb incident solar light. The solar cells positioned at the edges of these waveguides subsequently gather the photons that are emitted by the luminescent materials and are then trapped in the waveguide by total internal reflection (TIR), concentrating the light and generating electricity as a result.[32] Such devices offer the potential to significantly lower the solar cell size and equipment costs. However, because the surrounding chromophores may reabsorb the produced photons during the multiple internal reflection process, the performance of the currently used LSCs-based technologies is limited due to reabsorption losses.[33] Due to the tiny Stokes shift, traditional chromophores utilised in LSCs, such as coumarins and rhodamines, typically have planar conjugated structures and experience concentration quenching as well as self-absorption.[34] A prevalent solution to this issue is to either reduce the concentration of chromophores, but it means that less light can be absorbed by the LSCs[35] or a more effective approach is to use materials having large Stoke's shift. ESIPT-based LC materials, with visible-light emission from UV excitation, can be proven to be a great substitute of currently used materials in such devices due to their superior luminescent properties and large Stokes shift. Different molecules that exhibit mesogenic behavior in different phases such as nematic, smectic, *etc*. with ESIPT emission have been synthesized.[36–38] Among different mesophases, the columnar LCs (Col LCs) are widely known for their usefulness in a wide variety of applications including room-temperature OLEDs with blue and green emissions,[39–43] photovoltaic devices,[44–46] and optical compensation films for wide viewing display devices.[47,48] A π-electron-rich aromatic core surrounded by flexible alkyl chains comprises the fundamental structure of these mesogens that facilitates the charge carrier mobility within the aromatic cores in the stacks coupled *via* π–π interactions. A vast literature is available focussing on the efforts made for manipulating the charge transportation in Col LCs by the incorporation of a large variety of organic, inorganic and nanostructured dopants.[49–58] In addition to these electrical properties, other optical properties of LCs, including their photoluminescence (PL) properties play a crucial role in determining the efficacy of these materials. For this purpose, investigations in coupling the ESIPT activity with Col LC behaviour have been initiated, and the first breakthrough occurred in this direction when J. Seo *et al.* reported the synthesis of phasmidic LCs, forming J-type stacking in Col LC phases that exhibit ESIPT activity with a quantum yield of about 34% and Stokes shift up to 173 nm.[59] Afterwards, a homologous series of novel phasmidic bis(*N*-salicylideneaniline) Col LCs were synthesized by Kankala *et al.*, which exhibits hexagonal columnar (Col_h) phase with *p6mm* symmetry and are capable of providing dual fluorescent emissions through ESIPT.[60] To the best of our knowledge and within the light of the available literature, the modulation of the fluorescence emission of such compounds has not yet been performed but is of great importance as discussed earlier. This serves as the main motive behind this work. The present study has been focused on tuning the fluorescence emissions of one of the members of this phasmidic bis(*N*-salicylideneaniline)-based homologous series of Col LCs synthesized by Kankala *et al.*[60] To provide a comprehensive overview, two different organic dyes, namely, methyl red crystals (MRC) and rubrene, and two inorganic quantum dots (QDs) [carbon quantum dots

(CQDs) and cesium lead bromide ($CsPbBr_3$) perovskite quantum dots (PQDs)] have been doped into the host Col LC matrix for color tuning and modifying the PL emission behaviour. The exotic properties of these dopants have been briefly discussed in the subsequent sections to explain the reason behind choosing them for this study.

A quantum dot is a semiconductor whose excitons are confined in all three spatial dimensions. As a result, they have properties that are between those of bulk semiconductors and those of discrete molecules. Being zero-dimensional, quantum dots have a sharper density of states than higher dimensional structures. As a result, they have superior transport and optical properties. One of the most important properties of QDs is their ability to tune their bandgap and therefore control over their light absorption and emission frequencies. This is done through the quantization of their energy levels. Hence, quantum dots have been chosen for tuning the fluorescence emissions in the current study. In particular, we have chosen cesium lead bromide ($CsPbBr_3$) perovskite QDs (PQDs) and carbon QDs (CQDs). Perovskite quantum dots are a novel and intriguing class of nanocrystals that have recently come to light. $CsPbX_3$ (X = Cl, Br, I) is one of the fully inorganic halide perovskite QDs that is receiving a lot of attention because of its considerable photovoltaic properties, high photoluminescence quantum yield (up to 90%), and extensively adjustable emission wavelength through the alteration of the lead halide concentration.[61] PQDs additionally make excellent choices for laser and LED display applications because of their high temperature stability and narrow-band emission (20 nm) caused by an increase in the bound states in comparison to the bulk material. For our research, the two different quantum dots serve in developing a better understanding of tunable fluorescence emission and aid in achieving a wide color tuning in host Col LC.[62] A new class of carbon nanomaterials called carbon quantum dots (CQDs) has received attention as an alternative to classic semiconductor quantum dots. CQDs belong to the category of biocompatible QDs. The desired properties of CQDs are low toxicity, environmental friendliness, affordability, photostability, increased electronic conductivity with favourable charge transfer, and similar ease of synthesis processes.[63,64] CQDs have been widely used in LEDs, biosensing, and bioimaging applications because of their aforementioned unique qualities. Because of their special benefits—such as ease of synthesis, strong photostability, good solution dispersibility, low toxicity with chemical inertness, and, most importantly, tunable luminous properties—CQDs smaller than 10 nm have drawn our attention.

Furthermore, apart from QDs, dyes are well-known for their superior optical properties. Keeping this in mind, for the second part of the study, we have chosen two organic dyes—methyl red crystals and rubrene. The former, methyl red, belongs to the greatest class of commercially significant family of azo chemicals including synthetic organic dyes with the azo (–N=N–) linking group. The structure of these compounds is often R–N=N–R′, where R and R′ are either identical or differently substituted aryl groups.[65] These dyes have an intrinsic color because of electron delocalization caused by aromatic substituents attached to each end of the azo group. Their extensive range of uses is made possible by their common traits, which include their ease and versatility of synthesis, various structures, and the ability to achieve distinctive and highly intense colors.[66] The scientific community is particularly interested in the methyl red (MR) dye because of its remarkable nonlinear qualities among many other azo dyes that are accessible. It has been suggested as a viable option for several LC-based devices[67–69] due to their exceptional optical qualities, excellent dissolution in the LC host, significant dichroic ratio, and elongated and rod-like molecular form.[70] The other organic dopant, rubrene, tetraphenyl analogue of tetracene, finds its application as an organic semiconductor. It is used as a raw material to create transistors based on rubrene single crystals with carrier mobility more than 10 $cm^2\ V^{-1}\ s^{-1}$.[71,72] Rubrene has attracted our great attention for this study because of its high electrical conductivity, high mobility, emission characteristics and its wide applicability in organic opto-electronic devices.[73]

To summarize, it is worth contemplating that the distinct ESIPT emissions associated with the Col LC features make them a profoundly excellent choice for a variety of photonic applications, including luminescent solar concentrators (LSCs), organic light-emitting diodes (OLEDs), biosensing, and bioimaging. Adjusting these systems' fluorescence outputs is a topic of both scientific and practical interest. The ability to tune the fluorescence properties of ESIPT-active liquid crystals and henceforth achieving the color tuning, is of great significance and has not been done so far using different QDs and organic dopants. The photo-physical properties of PBSANs are interesting in view of their technological utility since their fluorescence behaviour can be altered by changing the substituents around the core, as reported previously.[60] Here, the change in photophysical properties of such mesogens on account of the dispersion of different organic and inorganic dopants has been investigated. The use of organic and inorganic dopants for this purpose can be proven as an effective strategy for enhancing the tunability of the fluorescence properties of this material. The integration of ESIPT-active liquid crystals with organic and inorganic dopants allows for the precise control over their fluorescence properties. This control opens up new possibilities for the development of advanced technologies and devices that rely on fluorescence-based processes.

2. Materials and methods

2.1 Sample description

A phasmidic mesogen named as phasmidic bis(*N*-salicylideneaniline) (PBSAN-14) has been used as the host liquid crystalline material for this study. It comprises of a long rod-like core with lipophilic segments on either side. The one used here in the study possesses six terminal paraffinic tails. The details of the synthesis procedure of the LC under study have been reported by Kankala *et al.*[60] It is a non-discoid LC that exhibits a special Col_h phase by self-assembling itself. It exhibits the columnar

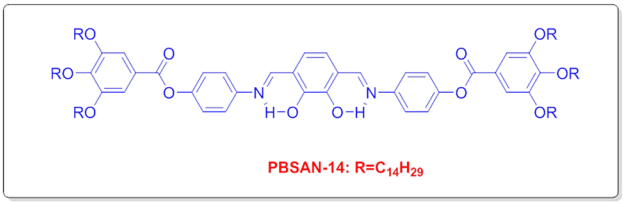

Fig. 1 Molecular structure of PBSAN-14.

mesophase in the temperature range between 82.9 °C and 127.8 °C. Under normal conditions, the LC exists in its *enol*-imine (OH) form and gets transformed into its *keto*-enamine (NH) form upon photoexcitation *via* tautomerism. The molecular structure of the host liquid crystal is provided in Fig. 1. The temperature-dependent XRD plot and the details of molecular packing and periodic parameters of the host LC can be found in Fig. S1 and Table S1, respectively (see ESI†).

For the study, two different organic dyes and two sets of inorganic quantum dots have been used. One of the two organic dopants is methyl red crystals (MRC), procured from Sigma-Aldrich (CAS no. 493-52-7). It is a member of the azobenzene family, a monocarboxylic acid and a tertiary amino compound, and has the chemical name 2-[[4-(dimethylamino)-phenyl]diazenyl]benzoic acid. The corresponding molecular formula is $C_{15}H_{15}N_3O_2$ with molecular weight = 269.30 g mol^{-1}. Its melting point is 182 °C. The other organic dopant chosen for this study is a red-colored polycylic aromatic hydrocarbon named as rubrene, purchased from Sigma-Aldrich (CAS no. 517-51-1). Its chemical name is 5,6,11,12-tetraphenyltetracene. Its chemical formula is $C_{42}H_{28}$ and melting point is 315 °C. The molecular structures of methyl red dye and rubrene are provided in Fig. S2 (see ESI†).

The two inorganic dopants, used in this study, are carbon quantum dots (CQDs) and cesium lead bromide ($CsPbBr_3$) perovskite quantum dots (PQDs). The organic-soluble carbon dots are of uniform size, about 7–8 nm in diameter. The detailed synthesis procedure of CQDs can be found in the article published by S. Kumar's group.[57] The $CsPbBr_3$ perovskite QDs were synthesized using the hot-injection method by P. Santra and his group. The $CsPbBr_3$ nanocrystals, with a standard orthorhombic structure, were of dimensions of about 8.6 ± 0.8 nm. The details of the synthesis procedure and high-resolution transmission electron microscopy (HRTEM) images for size confirmation can be found in the article published earlier.[74]

2.2 Experimental techniques

LC-dopant mixtures were prepared with the concentrations of both QDs fixed at 0.10, 0.25 and 0.50 wt% and the concentrations of organic dopants fixed at 0.5, 1.0 and 1.5 wt%. Above these concentrations, severe agglomerations could be observed, which is not desirable for the study. In order to prepare these composites, a predetermined weight of LC was mixed with an appropriate amount of a homogeneously dispersed dopant (0.1 mg mL^{-1}) in HPLC-grade dichloromethane (DCM) to achieve the required concentration. The temperature-dependent textural studies were carried out using a polarized optical microscope (Progress CT3 Radical, USA) equipped with Instec-mK 2000 to observe the change in the transition temperatures of the host LC due to doping. The UV-Vis spectra of the pristine LC and hybrid LC samples were recorded employing a PerkinElmer Lambda 750, 2015 NIR spectrophotometer. The fluorescence emission spectra were recorded using a Fluorolog-3, Horiba Jobin Yvon spectrofluorometer. The solution-state absorption and PL emission spectra were recorded by dispersing the composites in HPLC-grade DCM with concentration = 0.01 mg mL^{-1}. For the temperature-dependent photoluminescence studies, a Mettler Toledo HS82 hot stage controller was employed. The chromaticity coordinates and the corresponding chromaticity diagram were derived using the PL spectra with the help of the software Color-calculator (version 7.77), developed by OSRAM Sylvania Inc., United States.

3. Results and discussion

3.1 Mesomorphic behavior

The mesomorphic behavior of pristine PBSAN-14 and its composites were evaluated by polarized optical microscopy. To acquire information about the effect of doping different nanomaterials in varying concentrations, *i.e.*, change in transition temperatures, a minute quantity (~1 mg) of the sample was held between a glass slide and a cover slip, and it was subjected to repeated heating–cooling cycles using a hot plate. The observations from POM are illustrated in Fig. 2.

Upon heating, the samples undergo an endothermic phase transition from solid to mesomorphic state, characteristically displaying a fluid and homogeneous birefringent texture that remains unaltered until the isotropic point is reached. Upon cooling, a transition from the isotropic liquid state into Col_h occurs. The Col phase formed by the samples remains unaltered nearly up to room temperature (RT). The host sample shows a typical flower-like texture (spherulitic domains), which is also not affected due to doping. However, the transition temperatures were reduced since the dopants serve as impurities in the host LC. The corresponding data has been tabulated in Table 1.

3.2 Organic dyes in ESIPT-active LC host

Fig. 3(a) and (b) demonstrate the normalized UV-Visible absorption spectra for DCM solutions of pure PBSAN-14 with PBSAN-14/MRC and PBSAN-14/rubrene composites, respectively. Pure PBSAN-14 shows two absorption maxima at 275 nm and 360 nm, the latter being more intense as compared to the former one. The two absorption peaks can be assigned to n–π* and π–π* transitions, respectively. The dispersion of organic dopants leads to a decrease in the absorbance of the host LC, as is visibly clear from Fig. 3. In case of MRC-doped systems, the strong absorption of MRC in the visible region dominates as visible from the origin of a new absorption peak at 489 nm, resulting from the extended conjugation between the two

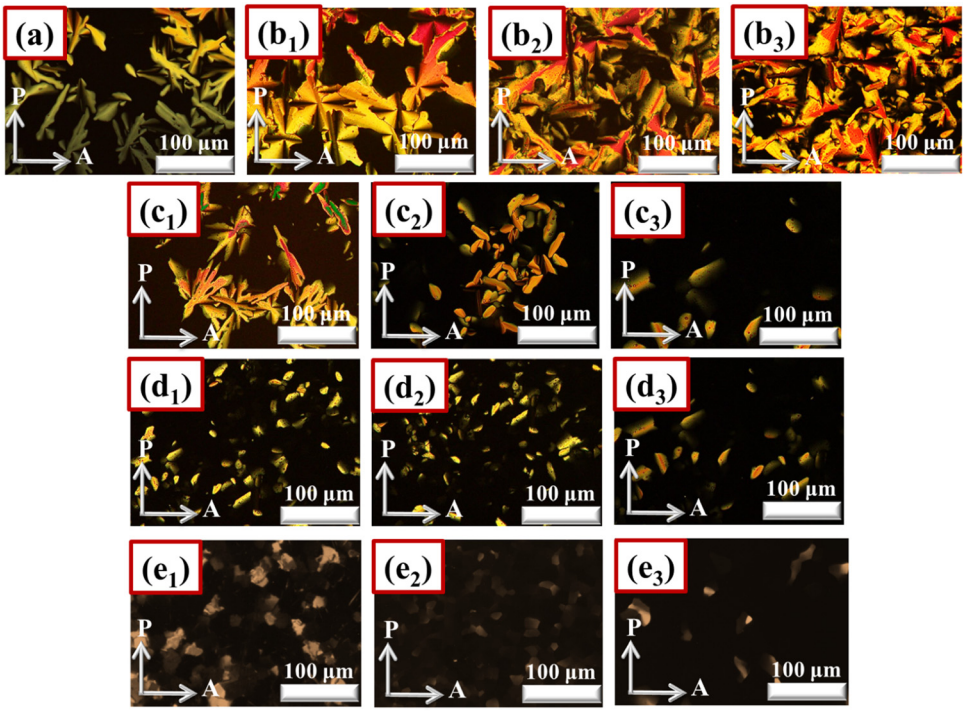

Fig. 2 POM images of thin films of the Col_h phase realized by (a) host PBSAN-14, (b_1)–(b_3) PBSAN-14/MRC composites, (c_1)–(c_3) PBSAN-14/rubrene composites, (d_1)–(d_3) PBSAN-14/CQDs composites and (e_1)–(e_3) PBSAN-14/PQDs composites.

Table 1 Thermal behaviour of pure and doped PBSAN-14 obtained using temperature-dependent textural acquisition (transition temperatures have been determined using temperature-dependent polarized optical microscopy)

	Phase transition temperatures (°C)	
Samples	Heating cycle	Cooling cycle
Pristine PBSAN-14	Cr 82.4 Col_h 127.1 Iso	Iso 124.7 Col_h
PBSAN-14 + 0.50 wt% MRC	Cr 82.0 Col_h 126.8 Iso	Iso 122.9 Col_h
PBSAN-14 + 1.00 wt% MRC	Cr 81.9 Col_h 125.1 Iso	Iso 121.7 Col_h
PBSAN-14 + 1.50 wt% MRC	Cr 80.7 Col_h 126.0 Iso	Iso 124.8 Col_h
PBSAN-14 + 0.50 wt% Rubrene	Cr 81.8 Col_h 126.2 Iso	Iso 124.1 Col_h
PBSAN-14 + 1.00 wt% Rubrene	Cr 81.5 Col_h 121.4 Iso	Iso 119.6 Col_h
PBSAN-14 + 1.50 wt% Rubrene	Cr 80.6 Col_h 117.2 Iso	Iso 115.9 Col_h
PBSAN-14 + 0.10 wt% CQDs	Cr 82.1 Col_h 126.1 Iso	Iso 123.5 Col_h
PBSAN-14 + 0.25 wt% CQDs	Cr 81.4 Col_h 123.4 Iso	Iso 121.2 Col_h
PBSAN-14 + 0.50 wt% CQDs	Cr 80.9 Col_h 122.1 Iso	Iso 119.9 Col_h
PBSAN-14 + 0.10 wt% PQDs	Cr 82.2 Col_h 125.6 Iso	Iso 123.1 Col_h
PBSAN-14 + 0.25 wt% PQDs	Cr 80.3 Col_h 123.4 Iso	Iso 120.9 Col_h
PBSAN-14 + 0.50 wt% PQDs	Cr 79.9 Col_h 120.8 Iso	Iso 118.4 Col_h

Abbreviations: Cr = crystal phase, Col_h = columnar hexagonal phase, Iso = isotropic phase.

units of chromophores. Similarly, in the case of dispersion of rubrene, for lower concentrations of rubrene in the host LC matrix, initially, the absorbance decreases but at higher concentrations, the peak at 360 nm gets strengthened along with a feeble absorption peak at about 290 nm, the characteristic absorption peak of rubrene. The UV-Visible and PL emission spectra for pure MRC and Rubrene are provided in Fig. S3 (see ESI†).

Under the 360 nm excitation wavelength, the pristine PBSAN-14 exhibits dual emissions at 430 nm and 615 nm; the former is ascribed to *enol*-emissions and the latter to *keto*-emissions in the ESIPT-active host system. The organic dopants MRC and rubrene produce fluorescence emissions peaked at 558 nm and 555 nm, respectively (Fig. S3, ESI†). The dispersion of organic dopants tends to decrease the intensity of fluorescence emissions of the host mesogen. For the quantitative analysis of the quenching behaviour, the temperature-dependent PL emission has been recorded for the thin films of pure and doped PBSAN-14. The results for the MRC-doped LC system are demonstrated in Fig. 4. The Stern–Volmer plots (S–V plots) of pristine and doped LC samples were examined to gain a better understanding of the mechanism of quenching.

In general, there are primarily, but not necessarily, two causes of quenching in the PL emissions of any composite, either due to the formation of non-fluorescent complexes due to ligand binding between the quencher and the material or due to the collision-driven non-radiative transitions; the former is termed as static, and the latter as dynamic quenching.[75] A linear correlation between the degree of quenching (F_0/F) and the concentration of quencher [Q] is presented by the S–V plot[76] and the governing equation has been provided below in eqn (1)

$$\frac{F_0}{F} = 1 + k_q\tau_0[Q] = 1 + K_{SV}[Q] \quad (1)$$

where F_0 and F denote the fluorescence intensities of the material in the absence and presence of quenchers, respectively, while k_q and K_{sv} signify the bimolecular quenching

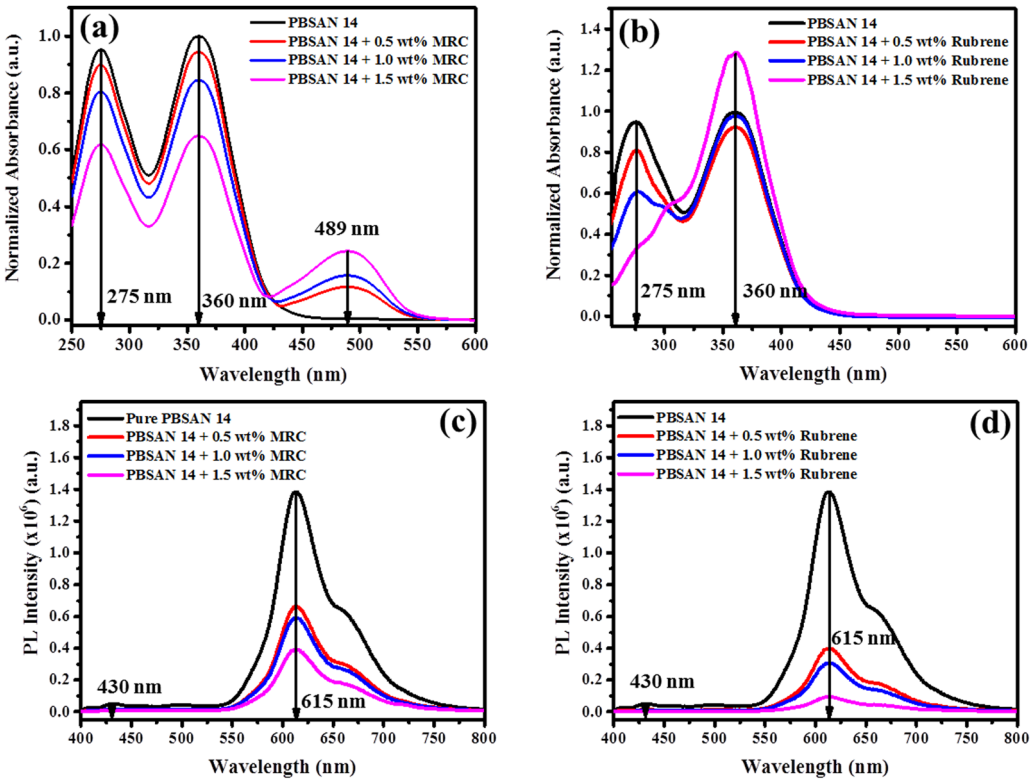

Fig. 3 UV-Visible absorption and fluorescence emission spectra for the solution state of (a), (c) PBSAN-14/MRC composites and (b), (d) PBSAN-14/rubrene composite.

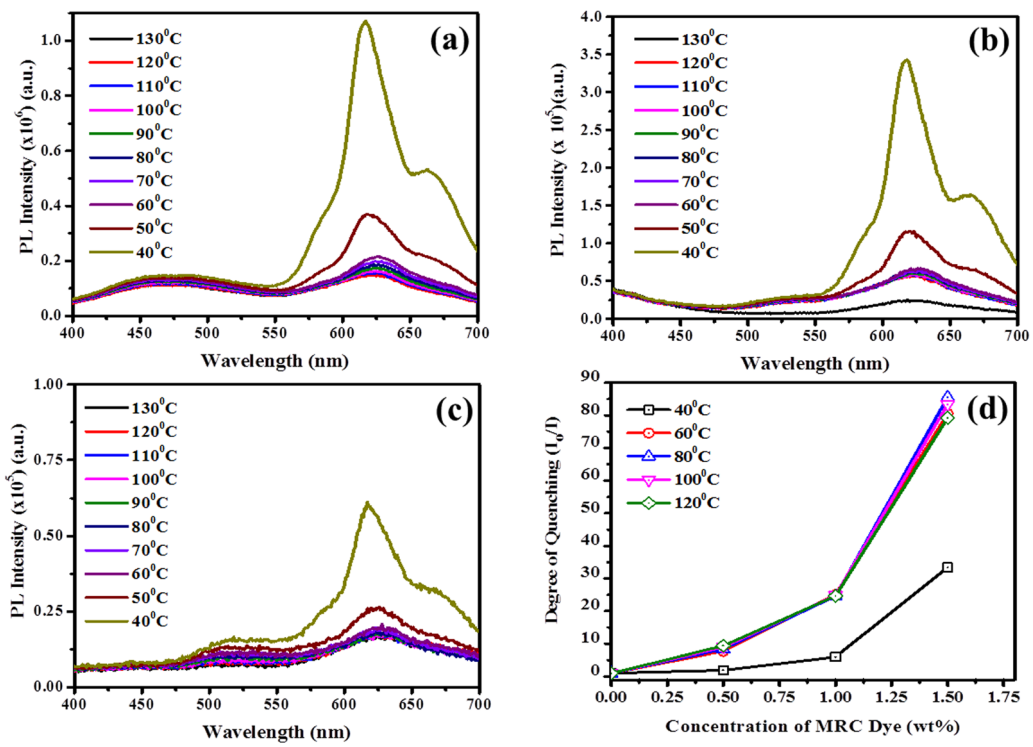

Fig. 4 Temperature-dependent PL spectra for thin films of (a) PBSAN-14 + 0.50 wt% MRC, (b) PBSAN-14 + 1.00 wt% MRC, (c) PBSAN-14 + 1.50 wt% MRC and (d) corresponding S–V plot for the PBSAN-14/MRC composites.

constant and Stern–Volmer quenching constant, respectively. The lifetime of the fluorophore in the absence of the quencher and the concentration of quencher is denoted by τ_0. For case of the PBSAN/MRC composites, the S–V plots have been depicted in Fig. 4(d). With increasing temperature, the S–V plots shift upwards and the concave curvature towards the vertical axis indicates the occurrence of collisional as well as static quenching together.[75]

A schematic of the model suggesting the mechanism of the quenching behavior has been illustrated in Fig. 5. The host LC molecules exist in their thermodynamically favoured *enol*-imine (OH) tautomeric form at the ground state E(S_0) under normal conditions. This is due to the presence of H-bridged, the quasi six-membered ring formed by the intramolecular H-bonding between the hydrogen and nitrogen atom of the respective hydroxy and imine groups. On irradiating the PBSAN-14/MRC composites with electromagnetic (EM) radiation of suitable energy, the LC molecules get excited to their Franck–Condon (FC) state, from where they populate their *enol*-excited state $E^*(S_1')$ *via* internal conversion and vibrational relaxation. Most of the excited fluorophores undergo the ESIPT process, yielding the *keto*-excited state $K^*(S_1')$. The fluorophores that experience a retrieval back to their original *enolic* form provide a feeble PL emission at about 430 nm, which excites the dye (MRC) molecules to its excited state. Methyl red dye exists in its *trans* form at RT and shows an absorption peak at 489 nm.[77] The excited LC fluorophores in the state $K^*(S_1')$ come in contact with the excited dye molecules and tend to form a non-fluorescent complex molecule that decays to attain its ground state without emitting any photon, thereby resulting in PL quenching with increasing concentration of MRC, to both static and collisional quenching occurring together. Moreover, it is clear from the Fig. 4 that for a particular concentration of MRC in the LC/MRC composite, the PL intensity also gets quenched with increasing temperature of the system because of thermally activated non-radiative transitions.

Henceforth, it is clear that the organic dyes act as fluorescence quenchers in the host mesogens. Due to this, the ESIPT activity gets interjected because of the interactions between the two moieties that results in a decrease in the fluorescence intensity of the composites, as discussed above.

3.3 Inorganic QDs in ESIPT-active LC host

UV-Visible spectroscopy was performed on the pristine and different QDs-dispersed PBSAN-14 in the solution state (using the DCM as a solvent), and the corresponding spectra has been depicted in Fig. 6 (Fig. 6(a) for PBSAN-14/CQDs composites and Fig. 6(b) for perovskite QDs-dispersed LC samples). The CQDs exhibit large absorption over the UV band with the tail extending towards the visible region and shows an absorption peaks at 350 nm and 410 nm (see ESI;† Fig. S3). These peaks are attributed to n–π* transitions of the C=O and surface state transitions involving electron lone pairs of the carbonyl bonds, respectively.[64] The perovskite QDs display a broad absorption spectrum and exhibit two absorption maxima at 357 nm and 506 nm (see ESI;† Fig. S3).

The host LC shows two absorption peaks at 275 nm and 360 nm, as discussed earlier in Section 3.2. With the dispersion of QDs in the host system into various percentages of weight ratios, the absorption peak situated at 275 nm gets shifted towards lower energy side (*i.e.*, longer wavelength at 300 nm), as apparent from Fig. 6(a). Weak dipole–dipole interaction between the LC molecules due to the dispersion of QDs might be a probable reason for this wavelength shift in the absorption spectra since a system requires less absorption energy if the dipole–dipole interaction is weak; henceforth, the spectrum gets shifted towards the longer end.[78,79] The decrease in the absorbance of the systems might be caused by the scattering of incident light.

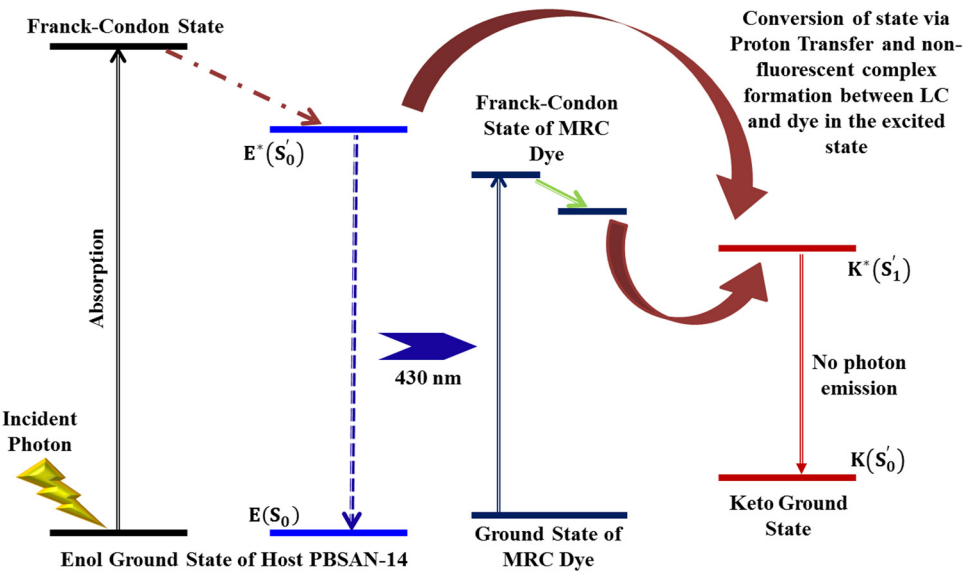

Fig. 5 Suggestive model in order to explain the mechanism of quenching on the dispersion of MRC dye in the host Col LC PBSAN-14.

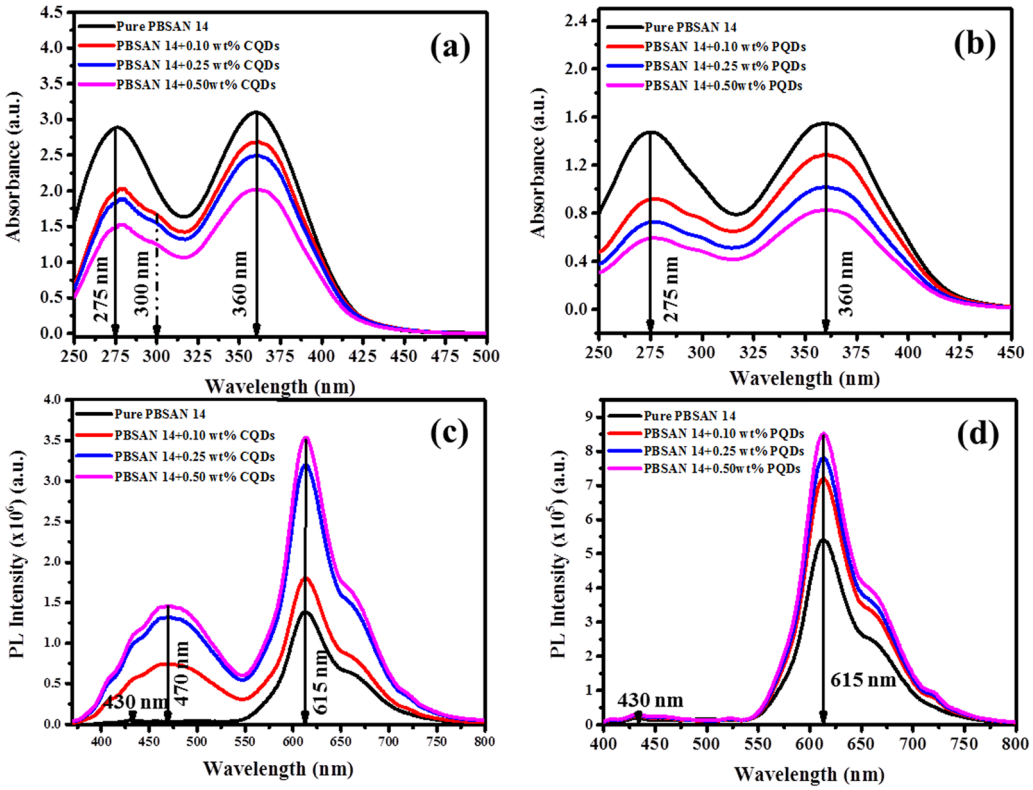

Fig. 6 UV-Visible absorption spectrum for (a) PBSAN-14/CQDs composites, (b) PBSAN-14/PQDs composites, Photoluminescence emission spectrum for (c) PBSAN-14/CQDs composites, (d) PBSAN-14/PQDs composites (in solution state).

The PL emission spectra for CQDs and PQDs-dispersed Col LC PBSAN-14 have been recorded in the solution state and illustrated in Fig. 6(c) and (d), respectively. Let us start the discussion with PQDs-dispersed LC composites. The dispersion of perovskite QDs, in various percentages, leads to a significant enhancement (around 2-fold intensification) of the PL emission intensity of the composites owing to the excellent fluorescent properties of the perovskite QDs.

On the dispersion of CQDs in the host LC, the obtained PL emission spectra shown in Fig. 6(c) shows a significant bathochromic shift of 40 nm in the first emission peak (corresponding to *enol* emissions) from 430 nm to 470 nm. Also, the PL emission spectrum gets significantly widened and enhanced with increasing percentage of CQDs and covers almost the entire visible region of EM radiation. The reason behind this red-shift in the enol emissions can be understood as follows: excitation energy of a suitable wavelength (360 nm) is incident upon the DCM solutions of PBSAN-14/CQDs composites. The excitation energy is sufficient to disrupt the state of equilibrium between the fluorophores and solvent dipoles. In order to achieve stabilization, the solvent molecules rotate themselves and get aligned with the excited fluorophores' dipoles. This tends to reduce the interaction energy of the system. Since this rotation occurs much ahead of fluorescence, it leads to the fluorescence emission spectrum getting red-shifted for the *enol*-emissions. Meanwhile, the position of *keto*-emission wavelength is not affected much. Furthermore, the increase in the CQDs in the host LC matrix facilitates the emission process and hence intensifies the emission spectrum.[64]

To further evaluate this result, the PL emission of the thin films of these composites has been recorded as a function of temperature and the results for pristine PBSAN-14, PBSAN-14/CQDs and PBSAN-14/PQDs composites are illustrated in Fig. 7(a)–(c), respectively. The spectra shown in Fig. 7(b) and (c) have been plotted for 0.10 wt% concentration of QDs only. The corresponding variations of the PL intensity of *keto* and *enol* emissions for the CQDs and PQDs-dispersed system has been illustrated in Fig. 7(d).

As it can be seen from Fig. 7(a), for the thin film of the pristine host mesogen, the PL emission spectra undergo a bathochromic shift of about 5 nm and 10 nm corresponding to the *enol*-form and *keto*-form, respectively. Furthermore, the intensity of *keto*-transitions tends to increase with a marginal red shift in the peak position of the emission maxima with decreasing temperature. Though, the intensity of both normal (corresponding to *enol*-form) and ESIPT emissions (corresponding to *keto*-form) gets enhanced on reducing the temperature, but the rate of increment is much higher for the ESIPT emissions. This change in the intensity as a function of temperature can be accredited to the breaking of larger aggregates or thermally-activated radiative transitions. The marginal red-shift in the spectra implies the formation of J-aggregates in the system. It occurs in the Col LC system when, within the columns, the π–π stacked aromatic cores

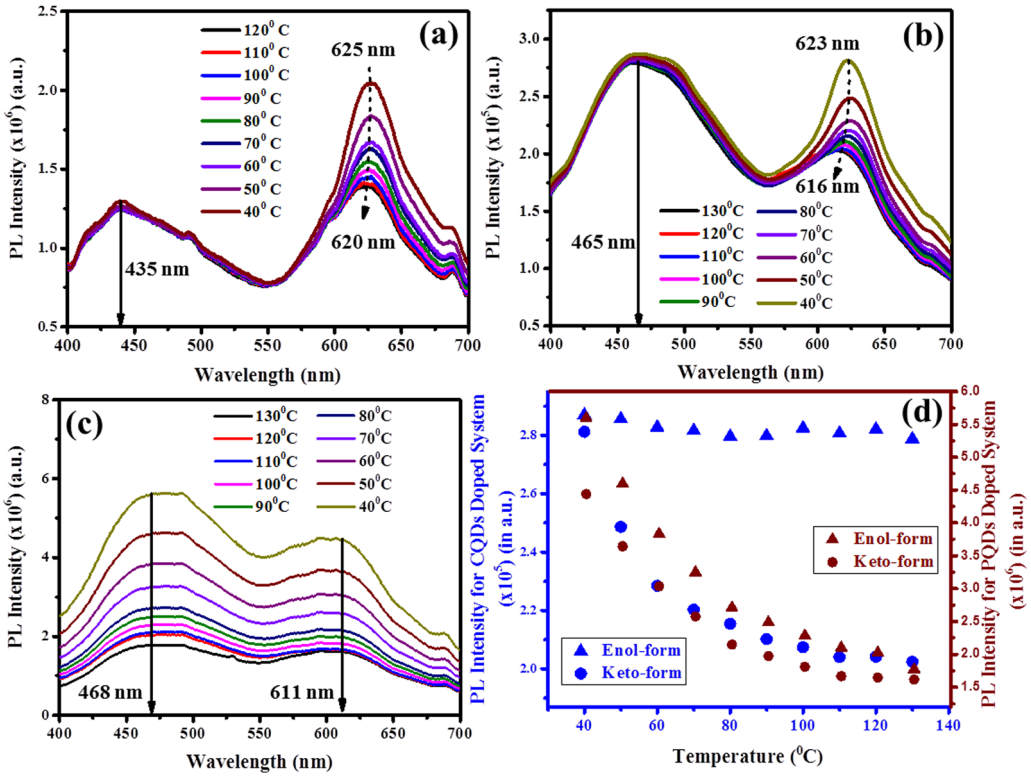

Fig. 7 Temperature-dependent photoluminescence spectrum for thin films of (a) pure PBSAN-14, (b) PBSAN-14 + 0.1 wt% CQDs composites, (c) PBSAN-14 + 0.1 wt% PQDs composites; (d) variation, as a function of temperature, of the PL intensity corresponding to the enol-form and keto-form for 0.1 wt% CQDs and PQDs-dispersed host hexacatenar matrix.

(oriented in head-to-tail manner) tilt with respect to the column axis.[60,80]

In case of PBSAN-14/QDs composites, as visible from Fig. 7(b) and (c), diminishing the fluorescence intensity can be seen for the *keto*-emissions due to QDs dispersion. This is due to the fact that the QDs tend to interrupt the process of intramolecular proton transfer in the host LC. The intensity of the *enol*-form decreases exponentially in case of the dispersion of both kinds of QDs, though the rate of decrease for the *keto*-form is quite different in both the cases. This quenching can be accredited to the thermal activation of non-radiative energy transfer pathways between the excited and ground state of the host LCs due to the insertion of

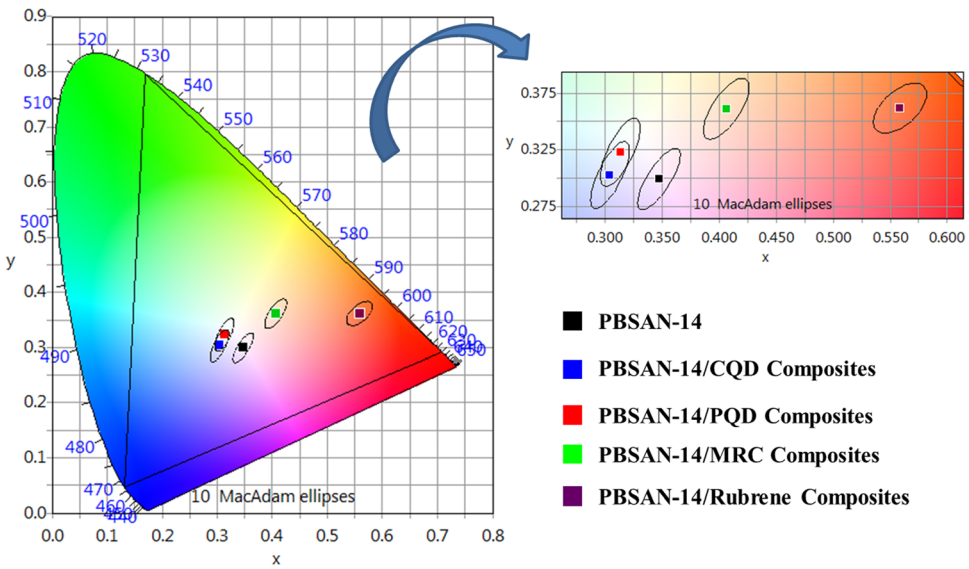

Fig. 8 Color tuning achieved in the host LC matrix on the dispersion of different organic and inorganic dopants.

Table 2 CIE coordinates corresponding to different composites

Composites	CIE coordinates
Pristine PBSAN-14	(0.3471,0.2994)
PBSAN-14 + Carbon QDs	(0.3042,0.3028)
PBSAN-14 + Perovskite QDs	(0.3132,0.3229)
PBSAN-14 + MRC Dye	(0.4062,0.3612)
PBSAN-14 + Rubrene	(0.5586,0.3618)

guest QDs, interrupting the proton transfer process and hence, reducing the ESIPT-emission intensity remarkably. However, it is worth mentioning that after the insertion of inorganic QDs into the host phasmidic Col LC, the system emits a continuous spectrum covering the entire visible range (400–800 nm), which serves as one of the most intriguing features of this study.

For the next generation of solid-state lightning sources, currently, white organic light-emitting diodes (WOLEDs) are drawing huge attention from both industry and academia. As a source of white light, an ideal WOLED should emit the entire visible regime of electromagnetic (EM) radiation. This can easily be achieved using such kind of mesogens. This would be discussed further in detail in the next section.

3.4 Color tuning outcomes

The alterations in the photoluminescence properties of the host phasmidic mesogen owing to the dispersion of different organic and inorganic dopants implies the possibility of achieving a wide range of color tuning by varying the dopant concentrations in the system. To evaluate this result, the ''International Commission on Illumination'' (CIE) coordinates have been derived from the photoluminescence spectra, and the corresponding CIE chromaticity diagram has been illustrated in Fig. 8. The corresponding coordinates for different dopants have been summarized in Table 2, which represents the color changes induced by the stimuli shown in Fig. 8.

One of the most favorable outcomes of these concentration-dependent experiments is that there is a slight change in the CIE coordinates of pure PBSAN-14 LC with the inclusion of different QDs and organic dyes in the system. As per the standards of European Broadcasting Union (EBU) and National Television System Committee (NTSC), the coordinates for white illuminant is (0.3333,0.3333). In our case, as is clear from Table 2, the coordinates with/without the dispersion of different dopants vary around this value, and the total luminescence color can be tuned over the whitish region and upto the red region by changing the kind of dopants used, as per the requirement in the device applications.

4. Conclusion

The mechanism of excited-state intra-molecular proton-transfer (ESIPT) has been widely used to develop versatile fluorescence probes and organic light-emitting diodes (OLEDs) due to the significant Stokes shift it can achieve. Currently, the available LSCs have limited applications due to the reabsorption losses by the chromophores due to the low Stokes shift. The adoption of ESIPT-active LC materials, which have the advantages of strong UV absorption, transparency and high emissivity in the visible region, and large Stoke's shift, is a fantastic endeavor to overcome such restrictions. ESIPT chromophores' fluorescence characteristics are influenced by a number of variables, including hydrogen bonds, substituents, and ambient circumstances. Understanding the fact that the ESIPT mechanism is crucial for the rational development of multifunctional luminescent materials, this novel study focuses on adjusting the fluorescence characteristics of ESIPT-active liquid crystals through the use of various inorganic and organic dopants. A columnar liquid crystal (Col LC) named phasmidic bis(*N*-salicylideneaniline) (PBSAN-14) has been dispersed with different organic (methyl red and rubrene) and inorganic dopants (carbon quantum dots (QDs) and $CsPbBr_3$ perovskite quantum dots). The dispersion of organic dyes such as methyl red crystals and rubrene quench the PL emissions of the host LC. Using S–V plots, the cause of quenching in the case of MRC was found to be the co-existence of static and dynamic quenching together. The formation of a non-fluorescent complex in the excited state during the collisions of the chromophores might have led to the quenched PL behaviour. On the contrary, the dispersion of quantum dots tends to facilitate the ESIPT process and enhances the fluorescence efficiency of the system. In the condensed state, thermally-activated non-radiative pathways reduces the intensity of *keto*-emissions owing to the transfer of energy between QDs and host mesogens. However, the solid-state emission spectra for PBSAN/QDs composites exhibit the PL emissions covering almost the entire visible regime. The CIE diagram shows a wide range of color tuning obtained by varying the type of dopant, as per the device requirement. The study provides a comprehensive overview over the effect of different organic and inorganic materials on the photo-physical properties of ESIPT-active LCs. It opens new opportunities for fundamental research and development in the field of ESIPT-active LCs nano-engineered in different ways in order to enhance their applicability for technical applications, since the development of highly emissive solid-state molecular materials have been grabbing great research interest in view of their applications in various solid state emitters, electroluminescent devices, luminescent solar concentrators (LSCs), organic laser, *etc.*

Author contributions

S. Agarwal: data curation, writing – original draft; S. Khatavi: formal analysis; B. P. Singh: review & editing; M. B. Kanakala: host LC synthesis; P. K. Santra: perovskite QDs synthesis and characterization; S. Kumar: carbon QDs synthesis and characterization; C. Y. Huang: resources (Organic Dopants); C. V. Yelamaggad: resources, conceptualization & methodology; R. Manohar: supervision, visualization.

Data availability

The data generated during and/or analysed during the current study are available from the corresponding author on reasonable request.

Conflicts of interest

The aforementioned authors wrote the original article and have approved its publication. They are aware of the content of the piece. This text is not presently being considered for publication elsewhere, and has never been published before. We also declare that, ''There is no conflict of interest.''

Acknowledgements

The authors acknowledge gratefully the Central Research Facilities, Centre for Nano and Soft Matter Sciences (CeNS), Bengaluru, for providing the necessary experimental facilities. Prof. Rajiv Manohar expresses his sincere gratitude to the state government of Uttar Pradesh for the Centre of Excellence (CoE) project at A. P. J. Abdul Kalam Innovation Centre and the Science and Engineering Research Board (SERB) for providing the research grant with File No. CRG/2021/006430. The authors are also grateful to Dr B. L. V. Prasad (Director, CeNS, Bengaluru) for his fruitful suggestions during the study.

References

1 A. Weller, *Naturwissenschaften*, 1955, **42**, 175–176.
2 A. Weller, *Z. Elektrochem.*, 1956, **60**, 1144–1147.
3 J. E. Kwon and S. Y. Park, *Adv. Mater.*, 2011, **23**, 3615–3642.
4 B. Dick and N. P. Ernsting, *J. Phys. Chem.*, 1987, **91**, 4261–4265.
5 S. Sinha, B. Chowdhury and P. Ghosh, *Inorg. Chem.*, 2016, **55**, 9212–9220.
6 G. J. Stueber, M. Kieninger, H. Schettler, W. Busch, B. Goeller, J. Franke, H. E. A. Kramer, H. Hoier and S. Henkel, *J. Phys. Chem.*, 1995, **99**, 10097–10109.
7 P. Chou, D. McMorrow, T. J. Aartsma and M. Kasha, *J. Phys. Chem.*, 1984, **88**, 4596–4599.
8 D. A. Yushchenko, V. V. Shvadchak, A. S. Klymchenko, G. Duportail, V. G. Pivovarenko and Y. Mely, *J. Phys. Chem. A*, 2007, **111**, 8986–8992.
9 M. Fischer and P. Wan, *J. Am. Chem. Soc.*, 1999, **121**, 4555–4562.
10 D. Yao, S. Zhao, J. Guo, Z. Zhang, H. Zhang, Y. Liu and Y. Wang, *J. Mater. Chem.*, 2011, **21**, 3568–3570.
11 H. C. Joshi and L. Antonov, *Molecules*, 2021, **26**, 1475.
12 M. Kasha, *J. Chem. Soc., Faraday Trans. 2*, 1986, **82**, 2379–2392.
13 A. J. Stasyuk, P. J. Cywiński and D. T. Gryko, *J. Photochem. Photobiol., C*, 2016, **28**, 116–137.
14 K.-i Sakai, S. Takahashi, A. Kobayashi, T. Akutagawa, T. Nakamura, M. Dosen, M. Kato and U. Nagashima, *Dalton Trans.*, 2010, **39**, 1989–1995.
15 J. Kumsampao, C. Chaiwai, C. Sukpattanacharoen, P. Nalaoh, T. Chawanpunyawat, P. Chasing, S. Namuangruk, N. Kungwan, T. Sudyoadsuk and V. Promarak, *Adv. Photonics Res.*, 2022, **3**, 2100141.
16 Z. Hu, H. Zhang, Y. Chen, Q. Wang, M. R. Elsegood, S. J. Teat, X. Feng, M. M. Islam, F. Wu and B. Z. Tang, *Dyes Pigm.*, 2020, **175**, 108175.
17 J. Cornil, D. Beljonne, J.-P. Calbert and J.-L. Brédas, *Adv. Mater.*, 2001, **13**, 1053–1067.
18 Z. R. Grabowski, K. Rotkiewicz and W. Rettig, *Chem. Rev.*, 2003, **103**, 3899–4032.
19 S. Kim, J. Seo and S. Y. Park, *J. Photochem. Photobiol., A*, 2007, **191**, 19–24.
20 H.-C. Peng, C.-C. Kang, M.-R. Liang, C.-Y. Chen, A. Demchenko, C.-T. Chen and P.-T. Chou, *ACS Appl. Mater. Interfaces*, 2011, **3**, 1713–1720.
21 W. Zhang, S. Suzuki, T. Sakurai, H. Yoshida, Y. Tsutsui, M. Ozaki and S. Seki, *Phys. Chem. Chem. Phys.*, 2020, **22**, 28393–28400.
22 T. Sakurai, M. Kobayashi, H. Yoshida and M. Shimizu, *Crystals*, 2021, **11**, 1105.
23 Y. Tsutsui, W. Zhang, S. Ghosh, T. Sakurai, H. Yoshida, M. Ozaki, T. Akutagawa and S. Seki, *Adv. Opt. Mater.*, 2020, **8**, 1902158.
24 L. Guo, M. Tian, Z. Zhang, Q. Lu, Z. Liu and X. Yu, *J. Am. Chem. Soc.*, 2021, **143**, 3169–3179.
25 L. He, B. Dong, Y. Liu and W. Lin, *Chem. Soc. Rev.*, 2016, **45**, 6449–6461.
26 J. Zhao, S. Ji, Y. Chen, H. Guo and P. Yang, *Phys. Chem. Chem. Phys.*, 2012, **14**, 8803–8817.
27 H. Gu, W. Wang, W. Wu, M. Wang, Y. Liu, Y. Jiao, F. Wang, F. Wang and X. Chen, *Chem. Commun.*, 2023, **59**, 2056–2071.
28 R. Reisfeld, *Sol-Gel Handb.*, 2015, 1281–1308.
29 F. Vollmer and W. Rettig, *J. Photochem. Photobiol., A*, 1996, **95**, 143–155.
30 A. Michalkiewicz, M. Kujawinska, J. Krezel, L. Salbut, X. Wang and P. J. Bos, Phase manipulation and optoelectronic reconstruction of digital holograms by means of LCOS spatial light modulator, *Eighth International Symposium on Laser Metrology*, SPIE, 2005, vol. 5776, pp. 144–152.
31 J. Kobashi, H. Yoshida and M. Ozaki, *Sci. Rep.*, 2017, **7**, 16470.
32 L. Wilson, B. Rowan, N. Robertson, O. Moudam, A. Jones and B. Richards, *Appl. Opt.*, 2010, **49**, 1651–1661.
33 A. Goetzberger and W. Greube, *Appl. Phys.*, 1977, **14**, 123–139.
34 C. Haines, M. Chen and K. Ghiggino, *Sol. Energy Mater. Sol. Cells*, 2012, **105**, 287–292.
35 M. G. Debije and P. P. C. Verbunt, *Adv. Energy Mater.*, 2012, **2**, 12–35.
36 W. Zhang, T. Sakurai, M. Aotani, G. Watanabe, H. Yoshida, V. S. Padalkar, Y. Tsutsui, D. Sakamaki, M. Ozaki and S. Seki, *Adv. Opt. Mater.*, 2019, **7**, 1801349.
37 V. S. Padalkar, Y. Tsutsui, T. Sakurai, D. Sakamaki, N. Tohnai, K. Kato, M. Takata, T. Akutagawa, K.-I. Sakai and S. Seki, *J. Phys. Chem. B*, 2017, **121**, 10407–10416.
38 C.-T. Liao, Y.-J. Wang, C.-S. Huang, H.-S. Sheu, G.-H. Lee and C. K. Lai, *Tetrahedron*, 2007, **63**, 12437–12445.
39 K. T. Kamtekar, A. P. Monkman and M. R. Bryce, *Adv. Mater.*, 2010, **22**, 572.

40 J. De, A. H. M. M, R. A. K. Yadav, S. P. Gupta, I. Bala, P. Chawla, K. K. Kesavan, J. H. Jou and S. K. Pal, *Chem. Commun.*, 2020, **56**, 14279–14282.
41 J. De, I. Sarkar, R. A. K. Yadav, I. Bala, S. P. Gupta, I. Siddiqui, J. H. Jou and S. K. Pal, *Soft Matter*, 2022, **18**, 4214–4219.
42 I. Bala, W.-Y. Yang, S. P. Gupta, J. De, R. A. K. Yadav, D. P. Singh, D. K. Dubey, J.-H. Jou, R. Douali and S. K. Pal, *J. Mater. Chem. C*, 2019, **7**, 5724–5738.
43 I. Bala, N. Singh, R. A. K. Yadav, J. De, S. P. Gupta, D. P. Singh, D. K. Dubey, J.-H. Jou, R. Douali and S. K. Pal, *J. Mater. Chem. C*, 2020, **8**, 12485–12494.
44 X. Feng, M. Liu, W. Pisula, M. Takase, J. Li and K. Mullen, *Adv. Mater.*, 2008, **20**, 2684–2689.
45 M. Kumar and S. Kumar, *Polym. J.*, 2017, **49**, 85.
46 J. Nelson, J. J. Kwiatkowski, J. Kirkpatrick and J. M. Frost, *Acc. Chem. Res.*, 2009, **42**, 1768–1778.
47 K. Kawata, *Chem. Rec.*, 2002, **2**, 59–80.
48 G. G. Nair, D. S. S. Rao, S. K. Prasad, S. Chandrasekhar and S. Kumar, *Mol. Cryst. Liq. Cryst.*, 2003, **397**, 245–252.
49 S. Kumar and V. Lakshminarayanan, *Chem. Commun.*, 2004, 1600–1601, DOI: **10.1039/b403794d**.
50 S. Orlandi, E. Benini, I. Miglioli, D. R. Evans, V. Reshetnyak and C. Zannoni, *Phys. Chem. Chem. Phys.*, 2016, **18**, 2428–2441.
51 R. Uttam, S. Kumar and R. Dhar, *Phys. Rev. E*, 2020, **102**, 052702.
52 Y. Shi, L. Tan and Y. Chen, *ACS Appl. Mater. Interfaces*, 2014, **6**, 17848–17856.
53 A. Gowda and S. Kumar, *Materials*, 2018, **11**, 382.
54 P. S. Kumar, S. Kumar and V. Lakshminarayanan, *J. Phys. Chem. B*, 2008, **112**, 4865–4869.
55 M. Kumar and S. Kumar, *RSC Adv.*, 2015, **5**, 1262–1267.
56 S. Kumar and L. K. Sagar, *Chem. Commun.*, 2011, **47**, 12182–12184.
57 P. Mahesh, A. Shah, K. Swamynathan, D. P. Singh, R. Douali and S. Kumar, *J. Mater. Chem. C*, 2020, **8**, 9252–9261.
58 A. Shah, B. Duponchel, A. Gowda, S. Kumar, M. Becuwe, C. Davoisne, C. Legrand, R. Douali and D. P. Singh, *New J. Chem.*, 2020, **44**, 14872–14878.
59 J. Seo, S. Kim, S. H. Gihm, C. R. Park and S. Y. Park, *J. Mater. Chem.*, 2007, **17**, 5052.
60 M. B. Kanakala and C. V. Yelamaggad, *J. Mol. Liq.*, 2021, **332**, 115879.
61 R.-S. Liu, *Phosphors, up conversion nano particles, quantum dots and their applications*, Springer, 2017.
62 X. Feng, X. Zhang, J. Huang, R. Wu, Y. Leng and Z. Chen, *Anal. Chem.*, 2022, **94**, 5946–5952.
63 A. S. Rasal, S. Yadav, A. A. Kashale, A. Altaee and J. Y. Chang, *Nano Energy*, 2021, 6515–6541.
64 S. K. Batabyal, B. Pradhan, K. Mohanta, R. R. Bhattacharjee and A. Banerjee, *Carbon Quantum Dots for Sustainable Energy and Optoelectronics*, Elsevier Science, 2023.
65 S. Benkhaya, S. M'rabet and A. El Harfi, *Heliyon*, 2020, **6**, e03271.
66 R. Christie, *Colour Chemistry*, Royal Society of Chemistry, 2nd edn, 2014.
67 S. Agarwal, B. P. Singh, S. Tripathi, P. Srivastava, S. Sharma and R. Manohar, *J. Phys. Chem. C*, 2023, **127**, 20466–20476.
68 M. Sheng, L. Zhang, S. Jiang, L. Yang, F. Zaaboul and S. Fu, *ACS Appl. Mater. Interfaces*, 2021, **13**, 13586.
69 M. Sheng, J. Li, X. Jiang, C. Wang, J. Li, L. Zhang and S. Fu, *ACS Appl. Mater. Interfaces*, 2021, **13**, 33282.
70 H. Seki, C. Shishido, S. Yasui and T. Uchida, *Jpn. J. Appl. Phys.*, 1982, **21**, 191.
71 V. Podzorov, E. Menard, A. Borissov, V. Kiryukhin, J. A. Rogers and M. E. Gershenson, *Phys. Rev. Lett.*, 2004, **93**, 086602.
72 H. Chang, W. Li, H. Tian, Y. Geng, H. Wang, D. Yan and T. Wang, *Org. Electron.*, 2015, **20**, 43–48.
73 B. W. Tao, W. X. Ming, H. Y. Lin, S. J. E, X. Z. Hui, W. Li and Y. S. Gen, *Chin. Phys. B*, 2014, **23**, 017803.
74 R. Rathod, R. Das, M. R. Das and P. K. Santra, *ACS Appl. Nano Mater.*, 2022, **5**, 9852–9860.
75 D. P. Singh, S. R. Inamdar and S. Kumar, in *Modern Techniques of Spectroscopy: Basics, Instrumentation, and Applications*, ed. D. K. Singh, M. Pradhan and A. Materny, Springer, Singapore, Singapore, 2021, pp. 431–468, DOI: **10.1007/978-981-33-6084-6_17**.
76 *Principles of Fluorescence Spectroscopy*, ed. J. R. Lakowicz, Springer, US, Boston, MA, 2006, pp. 277–330, DOI: **10.1007/978-0-387-46312-4_8**.
77 G. J. Lee, D. Kim and M. Lee, *Appl. Opt.*, 1995, **34**, 138–143.
78 J. R. Albani, *Principles and Applications of Fluorescence Spectroscopy*, 2007, pp. 115–123, DOI: **10.1002/9780470692059.ch8**.
79 J. R. Albani, *Principles and Applications of Fluorescence Spectroscopy*, 2007, pp. 88–114, DOI: **10.1002/9780470692059.ch7**.
80 A. S. Achalkumar, U. S. Hiremath, D. S. S. Rao, S. K. Prasad and C. V. Yelamaggad, *J. Org. Chem.*, 2013, **78**, 527–544.

